Math Geosci (2009) 41: 421–446
DOI 10.1007/s11004-008-9181-5

Deriving Optimal Exploration Target Zones on Mineral Prospectivity Maps

Pravesh Debba · Emmanuel J.M. Carranza · Alfred Stein · Freek D. van der Meer

Received: 2 June 2005 / Accepted: 13 June 2008 / Published online: 1 August 2008

Abstract This paper describes a quantitative methodology for deriving optimal exploration target zones based on a probabilistic mineral prospectivity map. The methodology is demonstrated in the Rodalquilar mineral district in Spain. A subset of known occurrences of mineral deposits of the type sought was considered discovered and then used as training data, and a map of distances to faults/fractures and three band ratio images of hyperspectral data were used as layers of spatial evidence in weights-of-evidence (WofE) modeling of mineral prospectivity in the study area. A derived posterior probability map of mineral deposit occurrence showing non-violation of the conditional independence assumption and having the highest prediction rate was then put into an objective function in simulated annealing in order to derive a set of optimal exploration focal points. Each optimal exploration focal point represents a pixel or location within a circular neighborhood of pixels with high posterior probability of mineral deposit occurrence. Buffering of each optimal exploration focal point, based on proximity analysis, resulted in optimal exploration target zones. Many of these target zones coincided spatially with at least one occurrence of mineral deposit of the type sought in the subset of cross-validation (i.e., presumed undiscovered) mineral deposits of the type sought. The results of the study showed the usefulness of the proposed methodology for objective delineation of optimal exploration target zones based on a probabilistic mineral prospectivity map.

P. Debba (✉)
CSIR, Logistics and Quantitative Methods, CSIR Built Environment, P.O. Box 395, 0001, Pretoria, South Africa
e-mail: pdebba@csir.co.za

P. Debba
e-mail: pdebba@gmail.com

E.J.M. Carranza · A. Stein · F.D. van der Meer
International Institute for Geo-Information Science and Earth Observation (ITC), Hengelosestraat 99, P.O. Box 6, 7500AA Enschede, The Netherlands

Keywords Simulated annealing · Epithermal deposits · Weights-of-evidence · Hyperspectral remote sensing · Hydrothermal alteration

1 Introduction

Occurrences of mineral deposits, which could be in the form of mines (economic and surveyed in three dimensions), prospects (surveyed mostly in two dimensions), or even showings (significant outcrops), are considered samples of a mineralized landscape. Occurrences of mineral deposits of the type sought are used for training in data-driven predictive mapping of mineral prospectivity. Basically, mineral prospectivity mapping involves delineating exploration targets, whereabouts the probability for the occurrence of the mineral deposit-type of interest is high. These targets might require a more detailed survey in a further stage of mineral exploration. In regional- to district-scale mineral prospectivity mapping, the objective is to delineate exploration target zones (i.e., polygons). This differs in local- to deposit-scale mineral prospectivity mapping, where the objective is to define exploration target locations or points.

Several mathematical methods exist for regional- to district-scale data-driven mapping of mineral prospectivity. Particular possibilities include the weights-of-evidence or WofE method (Good 1950; Bonham-Carter et al. 1988, 1989; Agterberg et al. 1990), logistic regression (Chung and Agterberg 1980; Agterberg and Bonham-Carter 1999), canonical favorability analysis (Pan 1993), neural networks (Porwal et al. 2003; Rigol-Sanchez et al. 2003), and evidential belief functions (Carranza and Hale 2003). Regardless of which data-driven method of mineral prospectivity mapping is applied, a logical question regarding the usefulness of a regional- to district-scale mineral prospectivity map in making a decision to proceed (or not to proceed) to the next higher scale of mineral exploration is: "Which areas of high likelihood of mineral deposit occurrence are optimal exploration target zones for further surveying of undiscovered occurrences of mineral deposits of the type sought?"

The objective of this paper is to demonstrate a methodology that we have developed in order to provide a plausible answer to the aforementioned question in a district-scale case study. We have tested our proposed methodology, for deriving optimal exploration target zones based on using a district-scale WofE-derived mineral prospectivity map of the Rodalquilar mineral district (southeastern Spain).

2 General Description of the Methodology

Initially, a mineral prospectivity map via the WofE method was created (Fig. 1). It was based on a Bayesian probability framework to update the prior probability of mineral deposit occurrences of the type sought in every unit cell or pixel in a study area. We used a set of training mineral deposit occurrences of the type sought and a number of thematic map layers of geological evidence having positive spatial association with these types of mineral deposits. The output mineral prospectivity map is a map of posterior probability of mineral deposit occurrences of the type sought. Using the map, we considered individual pixels to be prospective if their posterior probability

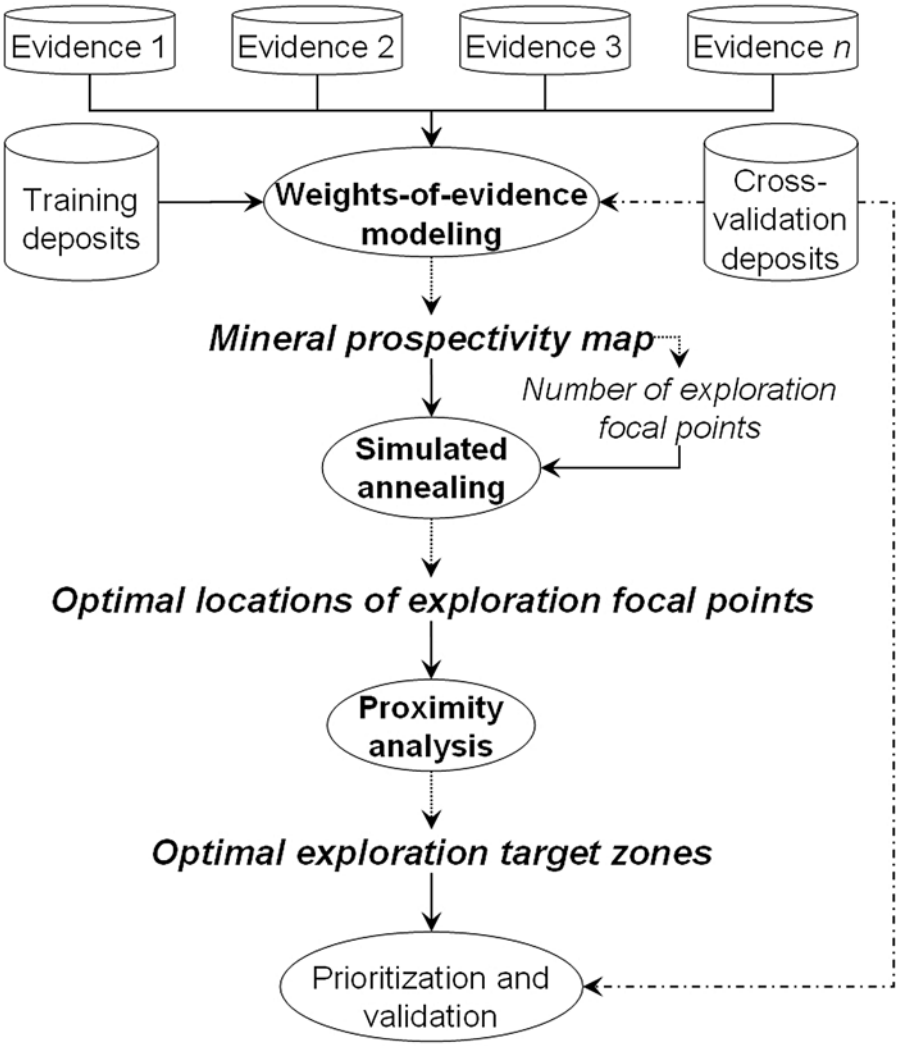

Fig. 1 A flow diagram outlining the stages to obtain the optimal exploration target zones

was greater than the estimated prior probability. After determining the prediction rate of the WofE-derived mineral prospectivity map (i.e., proportion of cross-validation deposits that coincide with prospective pixels), we used it as input spatial information for our proposed methodology (explained below), in order to determine the optimal exploration target zones. Although we used WofE to create a mineral prospectivity map in this case study, we postulate that any mineral prospectivity map derived by any of the methods mentioned earlier could also be useful for the same purpose.

In order to determine the optimal exploration target zones from a given mineral prospectivity map, we adopt the following paradigm. In searching for target object(s) of interest, not only in regional- or district-scale mineral exploration but also in other

types of "search endeavors" at similar scales (i.e., in large areas), one intuitively defines at first instance a focal point according to a set of criteria and then draws a perimeter (i.e., a search radius) around the focal point according to another set of criteria. The perimeter around the focal point is usually, but not always, circular within which to continue searching for the target object(s) of interest more intensively. Thus, with this intuitive paradigm, we used a WofE-derived posterior probability map in order to determine the optimal exploration target zones in the following way (Fig. 1). First, we used the prediction rate of the WofE-derived posterior probability map and the number of cross-validation deposits delineated correctly by the map in order to estimate a number of exploration focal points. For this purpose, we used the binomial distribution. Second, we used the posterior probabilities in the WofE-derived map and the estimated number of exploration focal points as input data and as a control parameter, respectively, in order to derive the locations of optimal exploration focal points. An optimal exploration focal point is a pixel or location, at and around which there is a high posterior probability of mineral deposit occurrences of the type sought.

Because mineral deposit occurrences are samples of a mineralized landscape, a configuration of exploration focal points can also be considered as a sampling scheme. Many studies have demonstrated that a sampling scheme can be optimized satisfactorily via simulated annealing (SA). Previous studies of SA applications to obtain optimal sampling schemes involved stratification of input data (van Groenigen et al. 2000a; Debba et al. 2008), definition of thresholds (van Groenigen et al. 2000a; Debba et al. 2005), definition of a weight function (van Groenigen et al. 2000b; Debba et al. 2005), and application of ordinary kriging (Shyan-Shu et al. 2005). Previous studies of deriving optimal sampling schemes in conjunction with remote sensing have used multispectral data (Tapia et al. 2005) or hyperspectral data (Debba et al. 2005, 2008). These studies typically developed model-based optimal sampling schemes (de Gruijter and ter Braak 1990). In this study, we demonstrate application of SA to derive a set of optimal exploration focal points based on a probabilistic mineral prospectivity map.

The optimal exploration focal points derived via the application of SA are then subjected to proximity analysis in order to delimit the optimal exploration target zones around each of them. Each of the optimal exploration target zones are prioritized according to certain criteria. The delineated optimal exploration target zones are then validated for each of the prioritized optimal exploration target zones and are tested against the set of cross-validation deposits that were also used to test and determine the prediction rate of the input WofE-derived posterior probability map (Fig. 1).

3 Generation of Prospectivity Map

3.1 Weights of Evidence (WofE) Modeling

WofE modeling (Good 1950; Bonham-Carter et al. 1988; Agterberg et al. 1990) is a Bayesian method that combines information from multiple layers of spatial evidences in order to predict the occurrence of a binary pattern. Each mineral deposit occurrence is treated as a binary object, being either present or absent, in every unit

cell or pixel. In mineral prospectivity mapping, each layer of spatial evidence has either a positive or negative spatial association with a set of training mineral deposit occurrences. Each layer of spatial evidence thereby either increases or decreases the posterior probability of mineral deposit occurrence at unvisited locations.

Let D represent a set of discovered mineral deposits with each deposit either contained in or represented by just one unit cell. Let $P(D)$ be an estimate of the prior probability of mineral deposit occurrence. Furthermore, let B^t denote a binary pattern of a layer of spatial evidence with a threshold at t, which is a spatial data attribute (e.g., band ratio or distance to faults/fractures), that is initially arbitrarily chosen. The conditional probability given the presence of B^t is

$$P\left(D|B^t\right) = P(D) \cdot \frac{P(B^t|D)}{P(B^t)}, \tag{1}$$

where $P(D|B^t)$ is the posterior probability of mineral deposit occurrence, given the presence of the binary pattern. Similarly, we can define the posterior probability of mineral deposit occurrence, given the absence of the binary pattern, $\overline{B^t}$.

In WofE, the posterior probability is converted to the posterior odds ratio ($O(A) = P(A)/P(\overline{A})$ for any occurrence A), by dividing both sides of (1) by $P(\overline{D}|B^t)$ and simplifying by replacing $P(\overline{D}|B^t) \cdot P(B^t) = P(B^t|\overline{D}) \cdot P(\overline{D})$. This yields

$$O\left(D|B^t\right) = O(D) \cdot \frac{P(B^t|D)}{P(B^t|\overline{D})}, \tag{2}$$

where $O(D|B^t)$ is the posterior odds of D given B^t and $O(D)$ is the prior odds of D. By taking the natural logarithm on both sides of (2),

$$\ln O\left(D|B^t\right) = \ln O(D) + W^+, \tag{3}$$

where $W^+ = \ln \frac{P(B^t|D)}{P(B^t|\overline{D})}$ is the weight of evidence for the presence of B^t. Similarly, using the posterior probability of the mineral deposit occurrence given the absence of B^t, we arrive at

$$\ln O\left(D|\overline{B^t}\right) = \ln O(D) + W^-, \tag{4}$$

where $W^- = \ln \frac{P(\overline{B^t}|D)}{P(\overline{B^t}|\overline{D})}$ is the weight of evidence for the absence of B^t.

The statistical significance of the weights can be determined based on their variances, which are approximated from Bishop et al. (1975) as

$$\begin{aligned} s^2(W^+) &= \frac{1}{N(B^t \cap D)} + \frac{1}{N(B^t \cap \overline{D})} \quad \text{and} \\ s^2(W^-) &= \frac{1}{N(\overline{B^t} \cap D)} + \frac{1}{N(\overline{B^t} \cap \overline{D})}, \end{aligned} \tag{5}$$

where $N(\cdot)$ denotes the number of counts. For example, $N(B^t \cap D)$ is the number of mineral deposit occurrences in the presence of the binary pattern B^t. Once

the weights W^+ and W^- are determined from (3) and (4) for each layer of spatial evidence B^t using several different thresholds, the maximum spatial contrast, $C = W^+ - W^-$ usually indicates the optimum threshold value of t, which can be calculated. If the number of mineral deposit occurrences is small, the studentized spatial contrast, $C/s(C)$ (where $s(C)$ is the standard deviation of C), aids in determining an optimum threshold value of spatial evidence in order to create B_i. The binary predictor maps, B_i, are then used to determine the posterior probability of the mineral deposit occurrence. For k sets of spatial evidence, resulting in $B_1, B_2, \ldots, B_k$ binary predictor maps,

$$P(D|B_1,\ldots,B_k) = \frac{P(B_1,\ldots,B_k|D)\cdot P(D)}{P(B_1,\ldots,B_k)} = \frac{P(B_1,\ldots,B_k|D)\cdot P(D)}{P(B_1,\ldots,B_k|D)\cdot P(D) + P(B_1,\ldots,B_k|\overline{D})\cdot P(\overline{D})}. \quad (6)$$

Equation (6) allows us to calculate the posterior probability of a mineral deposit occurrence given the presence or absence of an evidence. Because of their interaction, the terms $P(B_1,\ldots,B_k|D)$ and $P(B_1,\ldots,B_k|\overline{D})$ are difficult to estimate by the rules of probability, $P(D|B_1,\ldots,B_k)$ is biased, unless conditional independence (CI) is assumed among each of the $P(B_i|D)$ where $i = 1,\ldots,k$ binary predictor maps. Assuming CI, $P(B_1,\ldots,B_k|D) = \prod_{i=1}^{k} P(B_i|D)$. A similar expression applies for the second term in the denominator of (6). With k binary predictor maps, 2^k possible combinations of spatial evidence exist, depending on whether binary predictor map pattern B_i is present or not. This also means that there are 2^k unique conditions in the posterior probability map, being equivalent to 2^k polygons or grid cells in which the same combination of evidence occurs. After assuming CI in (6) and some simplifications, we obtain, in odds formulation,

$$\ln O_j(D|B_1,\ldots,B_k) = \ln O(D) + \sum_{i=1}^{k} W_i^j, \quad (7)$$

where W_i^j denote the weights (W_i^+ or W_i^-) contributed by spatial evidence in binary predictor map B_i ($i = 1, 2, \ldots, k$) to the jth unique condition ($j = 1, 2, \ldots, 2^k$). The posterior probabilities are then obtained from the posterior odds using

$$P_j = P_j(D|B_1,\ldots,B_k) = \frac{O_j(D|B_1,\ldots,B_k)}{1 + O_j(D|B_1,\ldots,B_k)}. \quad (8)$$

The variance of the posterior odds is

$$s^2(O) = \sum_{i=1}^{k} s^2(W_i), \quad (9)$$

where $s^2(W_i)$ is either $s^2(W_i^+)$ or $s^2(W_i^-)$ (defined by (5) for each binary predictor map B_i) depending on whether the binary predictor map B_i is present or not.

The images of the hyperspectral band ratios and the image of the distances to faults and fractures were converted to binary predictor maps B_i by finding the optimum threshold value in these images with respect to D in order to maximize positive spatial association of these evidential data with the target variable D as indicators of the mineral deposit occurrence. In the binary predictor maps, the corresponding values of W^+ and W^- are then assigned to the pattern indicating presence or absence of evidence, respectively. The binary predictor maps are then combined using (7) and the posterior probability is estimated using (8).

WofE modeling assumes CI among the evidence maps with respect to a set of the mineral deposit occurrences. Violation of this assumption causes the posterior probabilities to be over-estimated. The assumption of CI is tested using the 'new omnibus test' (NOT) (Agterberg and Cheng 2002; Thiart et al. 2004). The NOT compares the number of training mineral deposit occurrences $N(D)$ to the number of predicted training mineral deposit occurrences $N(D)_{\text{pred}}$, where

$$N(D)_{\text{pred}} = \sum_{i=1}^{2^k} P_j \{N(A)\}_j \tag{10}$$

and $\{N(A)\}_j$ is the area in unit cells for the ith unique condition. The test statistic (Agterberg and Cheng 2002; Thiart et al. 2004) under the null hypothesis $H_0 : N(D)_{\text{pred}} = N(D)$ is

$$\text{NOT} = \frac{N(D)_{\text{pred}} - N(D)}{s[N(D)_{\text{pred}}]}, \tag{11}$$

where the variance of the number of predicted training mineral deposit occurrences $s^2[N(D)_{\text{pred}}]$ is estimated by

$$s^2\big[N(D)_{\text{pred}}\big] = \sum_{i=1}^{2^k} \big[\{N(A)\}_j\big]^2 \times s^2(P_j) \tag{12}$$

and the variance of P_j is estimated based on the variance of the weights (Bonham-Carter et al. 1989) by

$$s^2(P_j) = \frac{1}{N(D)} + \sum_{i=1}^{k} s^2\big(W_i^j\big) \times P_k^2. \tag{13}$$

Values of NOT are assumed to approximate the standard Gaussian distribution and the hypothesis will be rejected in favor of $H_1 : N(D)_{\text{pred}} > N(D)$ for a statistically larger difference. An integrated model showing non-violation of the CI assumption is then used to create a posterior probability map. The prediction rate of a posterior probability map is estimated as the proportion of the predicted undiscovered mineral deposit occurrence in a cross-validation set. This corresponds with prospective pixels (i.e., pixels with posterior probability greater than the prior probability) in a WofE model created by using a training set of discovered mineral deposit occurrences. By

interchanging the roles of the two sets of mineral deposit occurrences as training and cross-validation data, the WofE model showing non-violation of the CI assumption and having the highest prediction rate is chosen as input to our proposed method for final derivation of the optimal exploration target zones.

3.2 Case Study

3.2.1 Geology and Mineralization of the Rodalquilar Mineral District

The Rodalquilar mineral district is located in the Sierra del Cabo de Gata volcanic field, in the south-eastern part of Spain (Fig. 2). It consists of pyroxene andesites to rhyolites of the late Tertiary age. Extensive hydrothermal alteration of the volcanic rocks resulted in the formation of high to low temperature minerals: silica → alunite → kaolinite → illite → chlorite. Occurrences of high- or low-sulphidation epithermal precious- and base-metal deposits are in veins or in hydrothermal breccias (i.e., fracture controlled) associated with hydrothermally altered rocks (Arribas et al. 1995). High-sulphidation precious-metal deposits are associated with advanced argillic (alunite ± kaolinite) and intermediate argillic (kaolinite ± illite) zones, whereas low-sulphidation precious- and base-metal deposits are associated with argillic to pyropylitic (illite ± chlorite) zones (Arribas et al. 1995). The epithermal minerals are localized along faults and fractures that cut through the volcanic host rocks. Based on these generalized geological characteristics of the discovered occurrences of epithermal mineral deposits in the district, we apply two recognition criteria in mapping prospectivity for epithermal mineral deposits: (1) hydrothermal alteration evidence, and (2) structural evidence.

3.2.2 Data for Hydrothermal Alteration Evidence

We used a sub-scene, consisting of 2640 × 1300 pixels, of airborne imaging spectrometer data acquired by the Hyperspectral Mapper (HyMAP) in July 2003 during

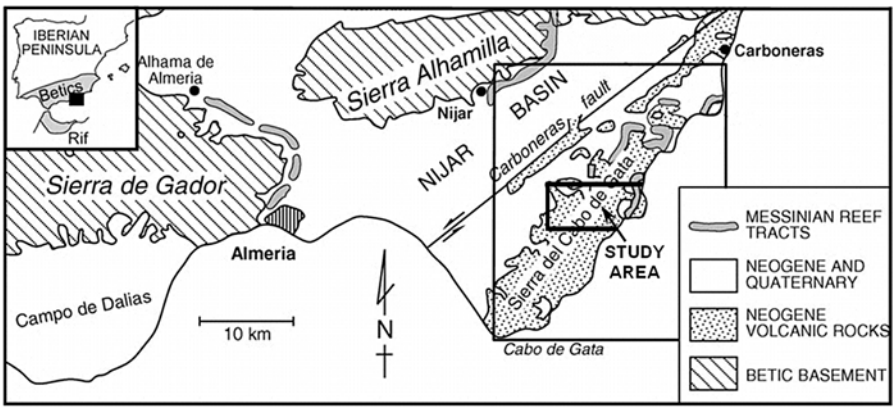

Fig. 2 A generalized geological map of the Rodalquilar area mineral district

the HyEUROPE 2003 campaign over the study area and its vicinity. HyMap is a 126-band sensor that collects spectral data in a cross-track direction by mechanical scanning and along-track direction by movement of the airborne platform. The HyMap sensor is an imaging spectrometer of reflected solar radiation within the 0.4–2.5 μm wavelength region of the electromagnetic spectrum. The spectral coverage of HyMap is nearly continuous in the visible-to-near-infrared (VNIR) and shortwave-infrared (SWIR) regions with small gaps in the middle of the 1.4 and 1.9 μm atmospheric water absorption bands. The spatial configuration of the HyMap sensor accounts for an instantaneous-field-of-view (IFOV) of 2.5 mrad along track and 2.0 mrad across track resulting in a pixel size of 3–5 m for the data used in this paper. Due to malfunction of the HyMap's SWIR 1 detector during acquisition, there was no data in the 1.50–1.76 μm spectral window. Data acquired by the SWIR 2 detector (bandwidth 16 nm), within the 1.95–2.48 μm spectral range was atmospherically and geometrically corrected using the Atmospheric and Topographic Correction (ATCOR 4) model (Richter 1996). The 1.95–2.48 μm spectral region covered the most prominent spectral absorption features of hydroxyl-bearing minerals, sulfates and carbonates, which are common to many hydrothermal alteration assemblages (Kruse 2002). SWIR 2 data was useful for mapping hydrothermal alteration assemblages as well as regolith characterization (Abrams et al. 1977; Goetz and Srivastava 1985; Cudahy et al. 2000; Kruse 2002).

Figure 3 shows the plots of spectra of seven most prominent hydrothermal alteration minerals in the study area (Arribas et al. 1995) at spectral intervals coinciding with the HyMAP SWIR 2 data. This figure shows the differences in absorption features of the different minerals, in terms of shape, size, symmetry, depth, and position. Other than the quartz spectrum, all the other spectra have distinctive absorption features at wavelengths of approximately 2.2 μm, although each absorption feature differs slightly in position and depth. In order to delineate predominant minerals in hydrothermal alteration zones associated with the epithermal deposits, hyperspectral band ratio images (Lillesand et al. 1994) were created using the HyMap SWIR 2 bands corresponding to the wavelengths indicated in Fig. 3, namely, bands 103/107 (2.100/2.171 μm), bands 107/109 (2.171/2.205 μm) and bands 118/112 (2.357/2.258 μm). Band ratioing is a way to enhance the presence of a material of interest from spectral images by dividing data in a spectral band with data in another spectral band. Band ratioing images can convey information, attributable to spectral properties of surface mineral, independent of variations in scene

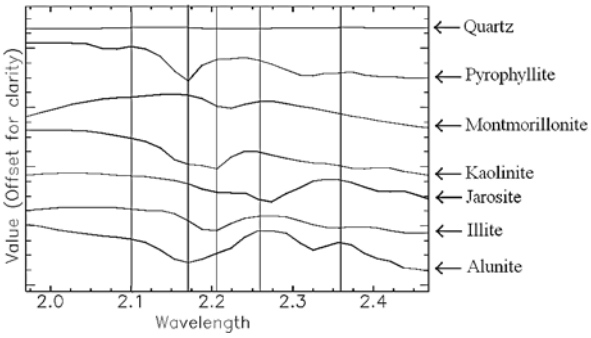

Fig. 3 Plot of seven endmembers from USGS spectral library (Clark et al. 1993) in the spectral range 1.95–2.48 μm. *Vertical lines* indicate the band centers used to obtain band ratio images (see text for further information)

illumination. We used an arctan transformation on the band ratios (Lillesand et al. 1994), which considered the gradient of spectral data between two bands.

Figure 4 displays the images of band ratios used as input evidence layers in WofE modeling. Pixels in the image of band ratio 1 (2.100/2.171 μm) are brighter (i.e., higher ratios) for alunite, kaolinite, and pyrophyllite but slightly darker (i.e., lower ratios) for illite (Fig. 4a). The first three minerals are predominant in advanced argillic zones. Pixels in the image of band ratio 2 (2.171/2.205 μm) are brighter for illite and kaolinite but are darker for alunite and pyrophyllite (Fig. 4b). The brighter pixels in the image of band ratio 2 thus enhance predominant minerals associated with intermediate argillic zones. Pixels in the image of band ratio 3 (2.357/2.258 μm) are darker for minerals predominant in advanced argillic zones but brighter for minerals predominant in argillic to pyropylitic zones (Fig. 4c).

3.2.3 Data for Structural Evidence

Mapped faults and fractures were screen-digitized on georeferenced raster-scanned maps, which were obtained from published (IGME 1981; Arribas et al. 1995) and unpublished sources. In addition, faults and fractures were interpreted and screen-digitized on shaded-relief images of a digital elevation model (DEM) derived from Advanced Spaceborne and Thermal Emission Radiometer (ASTER) data acquired on 26 May 2002. A map of distances to mapped and interpreted faults and fractures was then created (Fig. 4d) and used in WofE modeling.

3.2.4 Mineral Occurrence Data for WofE Modeling

Two sets of locations of mineral deposit occurrences were used in WofE modeling. One set, of 14 epithermal deposit occurrences, was digitized from a 1:50,000 scale geological map of Spain (IGME 1981) and from a map in Arribas et al. (1995). The other set, of 47 epithermal deposit occurrences, was digitized from the mineral prospectivity map of Rigol-Sanchez et al. (2003). This set actually shows 49 epithermal occurrences, although two of these fall outside our study area. In this latter set, 11 epithermal deposit occurrences were discarded because each of them lie within 25 m of an epithermal deposit occurrence in the first set, which indicates a high likelihood that these are the same 11 of the 14 in the first set. Thus, the second set has 36 epithermal deposit occurrences, each of which is believed to be different from the 14 epithermal deposit occurrences in the first set only in terms of location, but not in terms of deposit type. Each of the two sets of epithermal deposit occurrences were then used for training and for cross-validation of a WofE model. A training set is assumed to represent discovered mineral deposits, whereas a cross-validation set is assumed to represent undiscovered mineral deposits. The prediction rate was the criterion applied to select the better of the two WofE models created as input for derivation of optimal exploration zones. The epithermal deposit occurrences in either of the sets used are at present not economically interesting under the prevailing economic and geopolitical conditions. Thus, implications for the usefulness of the methods demonstrated here, based on either of these two deposit occurrence datasets, are discussed later.

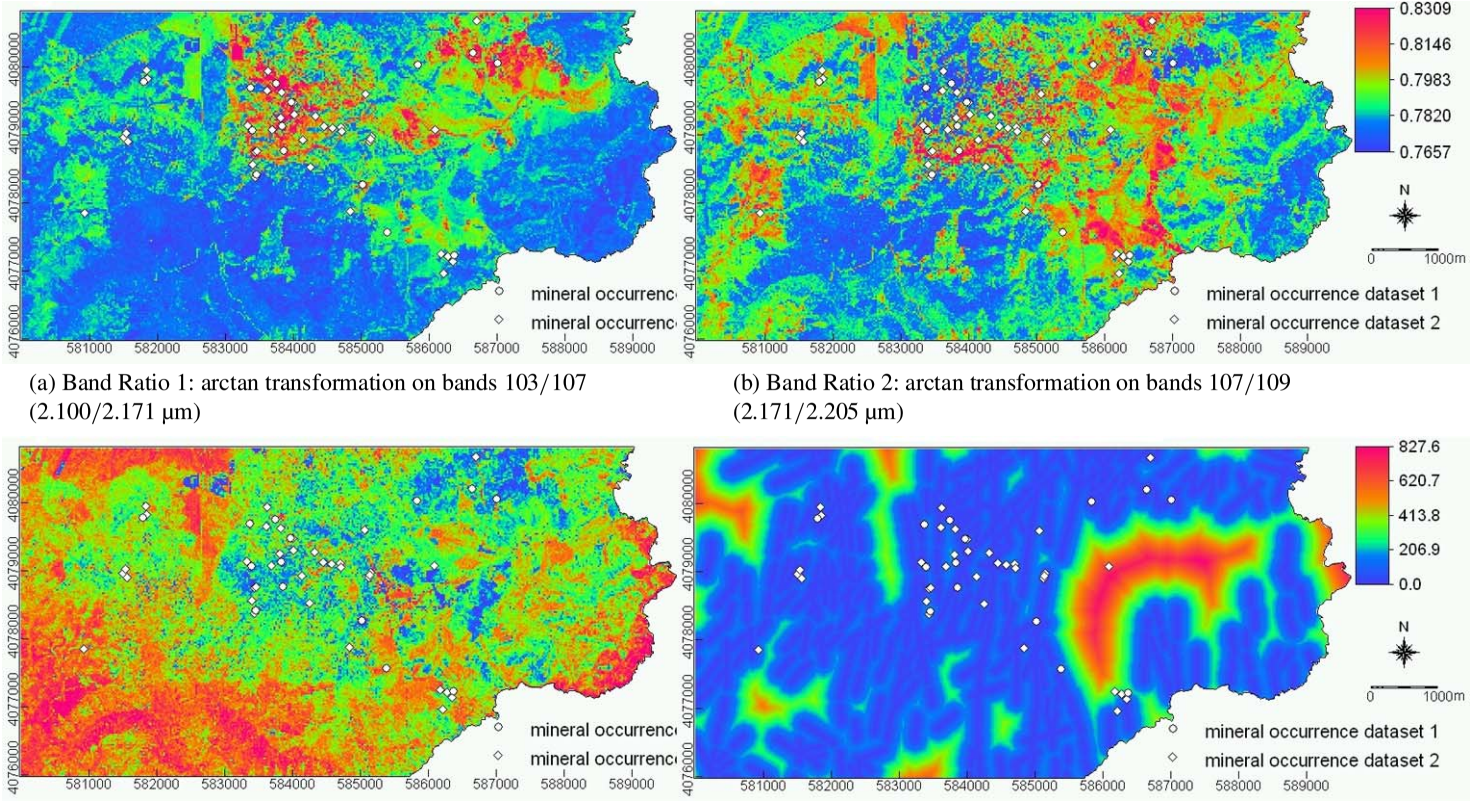

(a) Band Ratio 1: arctan transformation on bands 103/107 (2.100/2.171 μm)

(b) Band Ratio 2: arctan transformation on bands 107/109 (2.171/2.205 μm)

(c) Band Ratio 3: arctan transformation on bands 118/112 (2.357/2.258 μm)

(d) Distance to fault and facture. Increasing pixel brightness in this image indicates increasing distance from a fault or fracture

Fig. 4 Input layers for WofE modeling. Map coordinates are in meters (UTM projection, zone 30N)

3.3 Results of WofE Modeling of Mineral Prospectivity

The study area consists of 65253 unit cells of 25 × 25 m, based on the spatial resolution of the ASTER DEM. All the maps/images used in the analyses were resampled to this spatial resolution, which is adequately small and appropriate for WofE modeling (Agterberg 1992). Each unit cell or pixel containing a mineral deposit occurrence in training set 1 (with 14 epithermal occurrences) was buffered to a minimum of 25 m to increase the number of training set 1 pixels to 70 in order to obtain statistically significant weights and contrasts. The distance buffer, derived by point pattern analysis (Boots and Getis 1988), represents the minimum distance from each mineral deposit occurrence within which there is zero probability of another mineral deposit occurrence. The estimate of $P(D)$ based on training set 1 is 0.00107, whereas the estimate of $P(D)$ based on training set 2 is 0.00055. Table 1 shows the results of WofE modeling to create binary predictor patterns using the sets of hydrothermal alteration evidence and structural evidence with respect to either set of epithermal deposit occurrences.

Zones with high values of band ratio 1 (CR1) and band ratio 2 (CR2) have positive spatial associations with epithermal deposit occurrences in either set of the training data. Positive spatial association between zones with high values of CR1 and epithermal deposit occurrences is stronger than positive spatial association between zones

Table 1 Results of WofE calculations for binary predictor patterns based on range of spatial data attributes (in brackets under column 1) having optimum spatial associations (in terms of studentized C) with the training epithermal deposit occurrences

Binary predictor patterns[a]	$N(B)$[b]	$N(D \cap B)$[c]	W^+	$s(W^+)$	W^-	$s(W^-)$	C	Stud. C
Using training set 1 ($N(D) = 14$ epithermal deposit occurrences) for WofE modeling[d]								
CR1 (≥ 0.80)	13038	46	1.19	0.15	−0.85	0.20	2.04	8.10
CR2 (≥ 0.79)	32509	44	0.23	0.15	−0.30	0.20	0.53	2.16
CR3 (≥ 0.71)	52290	38	−0.56	0.18	1.01	0.16	−1.57	−5.97
DFF (≤ 70 m	24800	48	0.59	0.14	−0.68	0.21	1.27	4.55
Using training set 2 ($N(D) = 36$ epithermal deposit occurrences) for WofE modeling								
CR1 (≥ 0.81)	9819	19	1.26	0.23	−0.59	0.24	1.84	5.52
CR2 (≥ 0.79)	22791	19	0.41	0.23	−0.32	0.24	0.73	2.20
CR3 (≥ 0.70)	55419	21	−0.38	0.22	1.02	0.26	−1.39	−4.12
DFF (≤ 170 m	45396	32	0.25	0.18	−1.01	0.50	1.25	2.36

[a] Values in brackets indicate attributes of spatial data within pattern representing presence of binary evidence. CR1 = values of channel ratio 1 (Fig. 4a). CR2 = values of channel ratio 2 (Fig. 4b). CR3 = values of channel ratio 3 (Fig. 4c). DFF = distances to faults and fractures (Fig. 4d)

[b] Values in this column refer to number of pixels within pattern representing presence of binary evidence

[c] Values in this column refer to number of pixels of training data within pattern representing presence of binary evidence

[d] Each location of epithermal deposit was buffered to 25 m, which increased number of training pixels from 14 to 70

Table 2 Results of tests of the CI assumption based on NOT

Predictor map combination	NOT value	p(NOT)	CI test
Integrated models based on training set 1 ($N(D) = 14$ epithermal deposit occurrences) for WofE modeling			
CR1–CR2–CR3	1.77	0.038	Fail
CR1–CR2–DFF	0.49	0.312	Pass
CR1–CR3–DFF	2.09	0.018	Fail
CR2–CR3–DFF	1.00	0.159	Pass
CR1–CR2–CR3–DFF[a]	2.24	0.012	Fail
Integrated models based on training set 2 ($N(D) = 36$ epithermal deposit occurrences) for WofE modeling			
CR1–CR2–CR3	1.34	0.090	Pass
CR1–CR2–DFF	0.35	0.363	Pass
CR1–CR3–DFF	0.85	0.198	Pass
CR2–CR3–DFF	0.17	0.432	Pass
CR1–CR2–CR3–DFF	1.37	0.085	Pass

[a]CR1 = values of channel ratio 1 (Fig. 4a). CR2 = values of channel ratio 2 (Fig. 4b). CR3 = values of channel ratio 3 (Fig. 4c). DFF = distances to faults and fractures (Fig. 4d)

with high values of CR2 and epithermal deposit occurrences as indicated by the magnitude of W^+ and C. Zones with high values of band ratio 3 (CR3) have negative spatial association with epithermal deposit occurrences in either set of the training data. These results are consistent with field observations, as most epithermal deposits in the area are associated with intermediate argillic to advanced argillic alteration zones while some are associated with argillic to propylitic zones.

The epithermal deposit occurrences in training set 1 have a positive spatial association with faults and fractures, and the spatial association is optimal within 70 m of these geological features. The spatial association of faults and fractures with the epithermal deposit occurrences in training set 2 is also positive, and it is optimal within 170 m of these geological features. In training set 1, these results suggest that there is a higher proportion of vein-type epithermal deposits than disseminated-type epithermal deposits. In training set 2, there is a higher proportion of the disseminated-type epithermal deposits than the vein-type epithermal deposits. The types and relative strengths of spatial associations (as indicated by C or Studentized C) of the individual layers of spatial evidence with the epithermal deposit occurrences in set 1 and in set 2 are the same. This indicates that the epithermal deposit occurrences in either set 1 or set 2 have very similar geological characteristics. This implies further that a mineral prospectivity map derived through WofE modeling using either one of the two training sets would be able to predict a large proportion of epithermal deposit occurrences in the other set. Table 2 shows the results of the tests of CI on 3-layer and full 4-layer models of posterior probabilities of epithermal deposit occurrence based on each training set.

Only two 3-layer models based on training set 1 pass the NOT for CI assumption. The two 3-layer models exclusive of CR1 and CR3 both do not violate the CI assumption, whereas the models inclusive of CR1 and CR3 violate the CI assumption. Violation of the CI assumption is mainly due to overlap between the positive values in W^+ patterns of CR1 and the positive values in W^- patterns of CR3

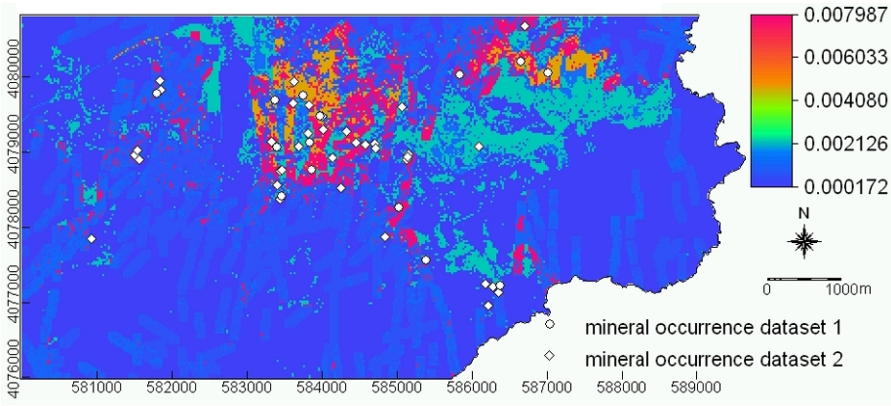

(a) Using training set 1 ($N(D) = 14$ epithermal deposit occurrences) for WofE modelling

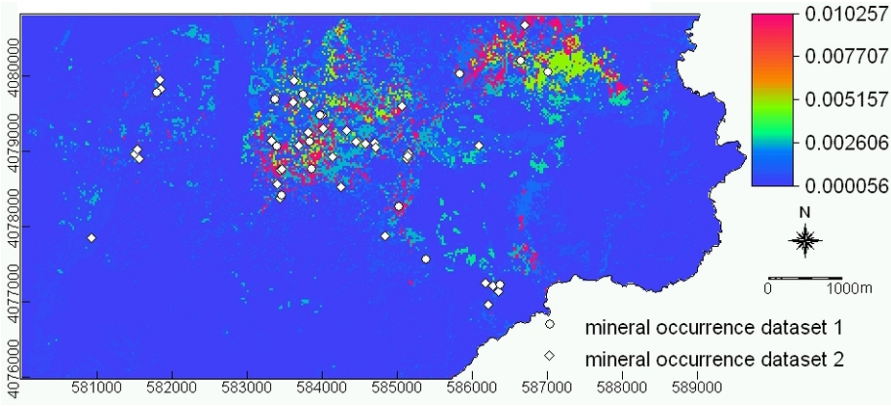

(b) Using training set 2 ($N(D) = 36$ epithermal deposit occurrences) for WofE modelling

Fig. 5 Maps of posterior probability of epithermal deposit occurrences

(Table 1), which results in an over-estimation of posterior probability. Each of the two 3-layer models, which pass the CI test, can be used mainly to map prospective zones for epithermal deposits associated with intermediate argillic to advance argillic zones. Based on prospective pixels, the CR1–CR2–DFF model has a prediction rate of 0.58 as it predicts correctly 21 of the 36 cross-validation deposit occurrences. The CR2–CR3–DFF model has a prediction rate of 0.47 as it predicts correctly 17 of the 36 cross-validation deposit occurrences. The posterior probability map based on the CR1–CR2–DFF model from training set 1 is shown in Fig. 5a.

All the 3-layer models and the full 4-layer model based on training set 2 pass the NOT for CI assumption. Models inclusive of CR1 and CR3, however, barely pass the NOT. This indicates to some degree the existence of a conditional dependence that the binary predictor patterns of CR1 and CR3 are to some extent conditionally dependent. This is mainly due to the overlap between the positive values in W^+ patterns of CR1 and the positive values in W^- patterns of CR3 (Table 1). Because all the integrated models based on training set 2 pass the CI test, each of them can be

used to map prospective zones for epithermal deposits. However, only the full 4-layer model was considered further in the analysis because it includes all of the four pieces or layers of spatial evidence, suggesting that it is useful not only for mapping zones prospective for epithermal deposits associated with intermediate to advanced argillic zones but also for epithermal deposits associated with argillic to propylitic zones. Based on prospective pixels and on training set 2, the CR1–CR2–CR3–DFF model has a prediction rate of 0.64 as it predicts correctly nine of the 14 cross-validation deposit occurrences. Thus, the full 4-layer model based on training set 2 is superior to any of the models based on training set 1. The posterior probability map based on the CR1–CR2–CR3–DFF model from training set 2 is shown in Fig. 5b.

3.4 Discussion on Predictive Modeling of Mineral Prospectivity

Deriving optimal exploration target zones depends on the accuracy of an input mineral prospectivity map, which in turn depends on the number and accuracy of evidential datasets. In the case of data-driven methods, it also depends on the number and accuracy of training data used in modeling. In the present work, we used four sets of evidential data and two sets of training deposit occurrences. Three sets of our evidential data are remotely-sensed data, which are indications of hydrothermal alteration. The accuracy of each set of remotely-sensed evidence is reliable based on a number of spectral measurements of ground samples used by Debba et al. (2005). Several other methods exist to detect hydrothermal alteration from spectral remote sensing data. For example, principal component scores from several spectral band ratio images (Crósta et al. 2003) could be used as evidence for the presence of hydrothermal alteration. However, with principal component analysis, it may be difficult to judge the hydrothermal alteration assemblages associated with the epithermal mineralization. Selecting pairs of hyperspectral bands for band ratioing in order to enhance the presence of hydrothermal alteration is more intuitive and practical than applying principal component analysis. The accuracy of interpreted faults/fractures, which were combined with the published mapped faults/fractures, was also considered reliable based on ground-checking.

The two sets of mineral deposit occurrences, used for training and cross-validation were each derived from independent published literatures (IGME 1981; Arribas et al. 1995; Rigol-Sanchez et al. 2003). The mineral deposit occurrences derived from the published literatures were considered accurate mainly in terms of their locations but not in terms of the deposit (sub-) type homogeneity. The rather low prediction rate (of 64%) of the probabilistic prospectivity map shown in Fig. 5b is attributable partly to the small number of evidential datasets used and to the presence of two (precious- and base-metal) sub-types of epithermal deposits used in modeling prospectivity. In regard to the latter, we could have prepared relatively homogeneous sets of training data precious-metal epithermal deposits by reclassifying all of the epithermal deposits in the district through an application of artificial neural network (Singer and Kouda 2003, 1997). However, the required datasets (e.g., mineralogy, grade and tonnages, etc.) for the classification of the mineral deposits via application of artificial neural networks were incomplete or unavailable. Alternatively, we could have combined the two mineral deposit occurrence datasets and then made a series of random

partitions into training and cross-validation data sets in order to carry out a bootstrap or jackknife validation, leading to the 'best' mineral prospectivity map. This was not an objective of this study. Instead our objective was to obtain a properly created and validated mineral prospectivity map with a good prediction rate based on limited available evidential data and mineral deposit occurrence data.

The 14 epithermal deposit occurrences in training set 1 are now mostly defunct mines and prospects, whereas the 36 epithermal deposit occurrences in training set 2 are mostly prospects and showings. The epithermal deposit occurrences in both sets are not economically interesting under the present economic and geopolitical conditions. In view of this, one might question the value of a mineral prospectivity map derived from using these training sets, in particular training set 2. The results of using these training sets, however, are consistent with results of previous works (Carranza and Hale 2000), where a larger training set of relatively non-economic deposit occurrences results in a mineral prospectivity model that is better than a mineral prospectivity model derived from a smaller training set of relatively economic deposit occurrences. The theoretical explanation for this is that 'non-economic' deposit occurrences have much higher frequencies, corresponding to a large number of samples, whereas 'economic' deposit occurrences have lower frequencies, corresponding to a small number of samples. Because mineral prospectivity mapping involves the concept of sampling, better mineral prospectivity models are more often derived when using larger number of samples than when using smaller number of samples. The two probabilistic prospectivity maps (Fig. 5) were created from two independently collected epithermal deposit occurrence data, and each map was validated with deposit occurrence data not used in modeling (Agterberg and Bonham-Carter 2005). The prospectivity map with the better prediction rate (Fig. 5b) was used as input data to the proposed method for deriving optimal exploration zones.

4 Derivation of Focal Points and Target Zones

In order to derive optimal exploration target zones, the posterior probabilities in a mineral prospectivity map are used (a) to estimate a reasonable number of exploration focal points (or pixels) and (b) as weights in an objective function to derive optimal exploration focal points via SA. Each of the optimal exploration focal points is then buffered with a reasonable distance determined via proximity analysis in order to derive a set of optimal exploration target zones.

4.1 Number of Exploration Focal Points

The number of exploration focal points must be estimated prior to deriving their optimal locations. Each optimal exploration focal point is represented by just one unit cell or pixel and is considered to be the centroid of a circular optimal neighborhood or zone of adjoining unit cells where the mineral deposit occurrence can be investigated further by an appropriate exploration technique. Since any optimal zone around each exploration focal point may or may not contain at least one undiscovered mineral deposit, the number of exploration focal points must be greater than or equal to

the number of undiscovered mineral deposits. Methods for estimation of the latter is discussed by Singer (1993). Here, we describe a procedure used for estimating the number of exploration focal points based on a mineral prospectivity map.

In order to estimate the number of exploration focal points, we employed a binomial distribution because the mineral deposit occurrence is a binary variable, being either present or absent. Thus, estimation of n exploration focal points so as to yield (or discover) at least r mineral deposit occurrences, with a probability of success p, at a 95% confidence, requires a solution for the following equation

$$\sum_{i=r}^{n} \binom{n}{i} p^i (1-p)^{n-i} = 0.95. \tag{14}$$

The obtained value of n from (14) is a way to determine the number of optimal exploration focal points. Each of the n optimal exploration focal points is a local optimum in a neighborhood of pixels where posterior probabilities are not only high but also having low uncertainty. Therefore, the optimal exploration focal points sought are non-adjoining pixels so that the assumption of independence among every n in (14) is not violated. Deriving the optimal exploration focal points requires definition of an objective function, called the fitness function.

4.2 Simulated Annealing

Simulated annealing is a generally applicable optimization technique for finding the global optimum of an objective function in the presence of local optima (Kirkpatrick et al. 1983; Bohachevsky et al. 1986). In SA, a fitness function $\phi(\mathbf{S})$, depending on the sampling configuration $\mathbf{S}$, has to be minimized. Starting with a random sampling scheme $\mathbf{S}_0$, let $\mathbf{S}_i$ and $\mathbf{S}_{i+1}$ represent two solutions with fitness functions $\phi(\mathbf{S}_i)$ and $\phi(\mathbf{S}_{i+1})$, respectively. Sampling scheme $\mathbf{S}_{i+1}$ is derived from $\mathbf{S}_i$ by randomly replacing one of the points of $\mathbf{S}_i$ towards a new point not in $\mathbf{S}_i$. A probabilistic acceptance criterion decides whether $\mathbf{S}_{i+1}$ is accepted or not

$$P_{\mathbf{c}}(\mathbf{S}_i \to \mathbf{S}_{i+1}) = \begin{cases} 1, & \text{if } \phi(\mathbf{S}_{i+1}) \le \phi(\mathbf{S}_i), \\ \exp\left(\frac{\phi(\mathbf{S}_i) - \phi(\mathbf{S}_{i+1})}{\mathbf{c}}\right), & \text{if } \phi(\mathbf{S}_{i+1}) > \phi(\mathbf{S}_i), \end{cases} \tag{15}$$

where $\mathbf{c}$ denotes a positive control parameter, usually called the temperature in SA problems. The parameter $\mathbf{c}$ is lowered, according to a cooling schedule as the process evolves, in order to find the global minimum. A transition takes place if $\mathbf{S}_{i+1}$ is accepted. Next, a solution $\mathbf{S}_{i+2}$ is derived from $\mathbf{S}_{i+1}$, and the probability $P_c(\mathbf{S}_{i+1} \to \mathbf{S}_{i+2})$ is calculated with a similar acceptance criterion as in (15). For each value of $\mathbf{c}$, several transitions have to be made before the annealing can proceed and $\mathbf{c}$ can take its next value.

A slow linear cooling schedule was chosen, in order to prevent solutions at local minima so that the chance of arriving at the global minimum increases. The cooling schedule starts with an initial value $\mathbf{c}_0$ which has an acceptance ratio (γ) of 0.95 or higher for alternative solutions. For $l = 0, 1, 2, \ldots$, the decrements of $\mathbf{c}$ is given by $\mathbf{c}_{l+1} = \gamma \cdot \mathbf{c}_l$, with $0 < \gamma < 1$.

For a two-dimensional region A divided into $N(A)$ unit cells, let the spatial configurations of n optimal exploration focal points be denoted by $\mathbf{S}^n$. We denote the posterior probability of the mineral deposit occurrence per unit cell in A derived from WofE modeling (i.e., A represents all prospective pixels) by $P(\vec{\mathbf{x}}) = \{P_j(\vec{\mathbf{x}})|\vec{\mathbf{x}} \in A\}$, where $\vec{\mathbf{x}}$ is the location vector of the unit cell in A, with a corresponding pixel in an image I, for unique condition j. A fitness function $\phi(\mathbf{S}^n) : \mathbf{S}^n \to \mathbb{R}^+$, which is an extension to the Weighted Means Shortest Distance (WMSD)-criterion (Debba et al. 2005; van Groenigen et al. 2000b), is minimized to optimize the search for n exploration focal points.

$$\phi_{\mathrm{WMSD+V}}(\mathbf{S}^n) = \frac{\lambda}{N(A)} \sum_{\vec{\mathbf{x}} \in A} P(\vec{\mathbf{x}}) \left\| \vec{\mathbf{x}} - Q_{\mathbf{S}^n}(\vec{\mathbf{x}}) \right\| + (1-\lambda) s^2(O_{\mathbf{S}^n}), \tag{16}$$

where $Q_{\mathbf{S}^n}(\vec{\mathbf{x}})$ is the location vector of an optimal exploration focal point in $\mathbf{S}^n$ nearest to $\vec{\mathbf{x}}$, and $s^2(O_{\mathbf{S}^n})$ is the variance of the posterior odds (9) at every optimal exploration focal point in $\mathbf{S}^n$. The spatial distribution of posterior probabilities expresses the knowledge or assumptions about the spatial distribution of mineral deposit occurrences in region A, while the magnitude of the posterior probabilities controls the selection of a unit cell or pixel as an optimal exploration focal point. A pixel with posterior probability higher than its neighboring pixels, therefore, is a candidate for selection as an optimal exploration focal point. The variance of the posterior odds also controls the selection of optimal exploration focal points in a neighborhood of pixels where the posterior probabilities are not only high but also have a low uncertainty. The objective function that was optimized by considering not only the magnitude of the posterior probability but also the uncertainty of the posterior probability. By doing so, optimal exploration focal points are spread over the district and positioned in pixels with high posterior probability and low uncertainty of coinciding with or being proximal to an undiscovered deposit (i.e., a deposit occurrence in the cross-validation set that is predicted correctly by the input WofE model of mineral prospectivity). This means that optimal exploration focal points are sited in areas characterized by strong and statistically significant positive spatial associations between evidential patterns and discovered (i.e., training set of) mineral deposit occurrences. The $\lambda \in [0, 1]$ is a constant controlling the effect of the posterior probability and the variance of the posterior odds in finding and selecting optimal exploration focal points. The value of λ could be estimated automatically by random selection between $[0, 1]$ when the above fitness function is minimized through SA.

4.3 Case Study

The posterior probability map (Fig. 5b) based on the training set 2 was used as input data to derive optimal exploration focal points. Training set 1 was used as a cross-validation set and a as reference for the number of undiscovered epithermal deposits (i.e., deposit occurrences in the cross-validation set that are predicted correctly by the input WofE model of mineral prospectivity) in order to validate the derived set of optimal exploration target zones.

4.4 Results of Deriving Optimal Exploration Target Zones

4.4.1 Estimated Number of Exploration Focal Points

In solving for n in (14), we first assumed that $r = 9$ based on the nine predicted out of 14 undiscovered epithermal occurrences in training set 1 and that $p = 0.0025$ based on the average posterior probabilities of prospective pixels in the input WofE prospectivity model. With these assumptions we derive $n = 6280$. This number of exploration focal points is intractable. However, we interpret and show later that 6280 is approximately the total number of unit cells within plausible exploration target zones. Instead of $p = 0.0025$, we used $p = 0.6$ based on the approximate prediction rate of the input WofE model. Accordingly, $n = 22$, which is a plausible number of exploration focal points as centroids of individual exploration target zones wherein to search further for the nine (assumed) undiscovered epithermal deposit occurrences.

4.4.2 Locations of Optimal Exploration Focal Points

By using the posterior probability map shown in Fig. 5b as input and by specifying $n = 22$ and $\lambda = 0.5$ in (16), the locations of the optimal exploration focal points were derived. The value of $\lambda = 0.5$ was chosen instead of being estimated automatically in order to avoid computational time problem and to specifically avoid giving preference to the effect of either the posterior probability or the variance of the posterior odds in the fitness function. Each of the derived optimal exploration focal points (Fig. 6) occupies a unit cell with the highest posterior probability value based on training set 2 in a circular neighborhood of unit cells with posterior probabilities greater than the prior probability estimate. This indicates that the algorithm was effective in finding and selecting optimal exploration focal points in prospective ground (i.e., adjoining prospective pixels). Each of the derived optimal exploration focal points does not fall exactly on but is proximal to a unit cell representing an undiscovered epithermal mineral deposit occurrence belonging to either set of epithermal deposit occurrence

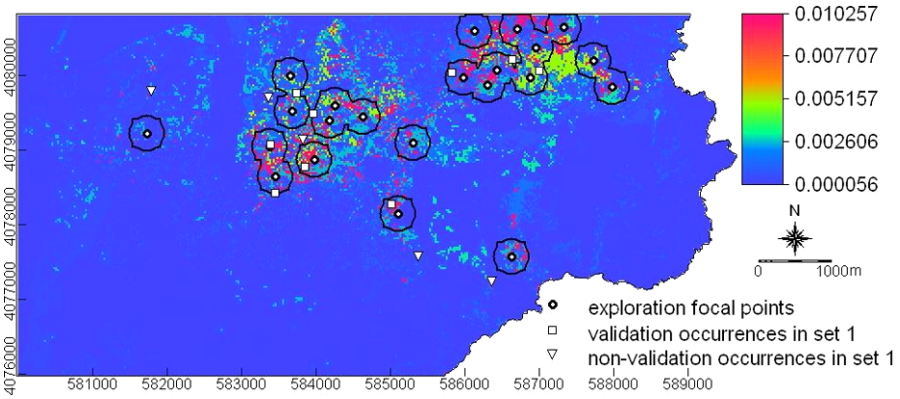

Fig. 6 Optimal exploration target zones defined by buffering to 238 m each of the optimal exploration focal points

data in training set 1. This is a validation occurrence predicted correctly by the input WofE model. Because the derived optimal exploration focal points are each considered to be the centroid of a circular neighborhood or zone of adjoining pixels where a mineral deposit occurrence could be explored at higher scales, exploration target zones should be delineated around them.

4.4.3 Optimal Exploration Target Zones

In order to define optimal exploration target zones around each of the derived optimal exploration focal points, the following analysis was performed. We quantified proximity to an undiscovered deposit occurrence by utilizing the estimated number of 6280 unit cells required to delineate the nine predicted deposit occurrences out of the 14 cross-validation deposit occurrences and using $p = 0.0025$ in (14). The total area represented by the 6280 unit cells is approximately $6280 \times 25^2 = 3925000$ m^2. If each of the nine undiscovered deposit occurrences, predicted by the WofE model, out of the 14 cross-validation undiscovered deposit occurrences, is within a delineated sub-area of $3925000/22 = 178409$ m^2 containing each of the optimal exploration focal points, then this indicates that an optimal exploration target zone is proximal to at least one undiscovered deposit occurrence. This also means that, if each of the nine predicted undiscovered deposit occurrences, delineated by the WofE model, out of the 14 cross-validation undiscovered deposit occurrences, is within a radius of $\sqrt{178409/\pi} = 238$ m (area of circle $= \pi \times$ radius^2) around a derived optimal exploration focal point, then an optimal exploration focal point is in close proximity to at least one undiscovered deposit occurrence.

Each of the 22 derived optimal exploration focal points was then buffered with a radius of 238 m in order to delineate optimal exploration target zones. Seven of the nine (assumed) undiscovered deposit occurrences, delineated by the WofE model out of the 14 cross-validation undiscovered deposit occurrences, are within the delineated optimal exploration target zones. The result of this analysis indicates that the derived optimal exploration focal points are proximal to undiscovered epithermal deposit occurrences. The average of posterior probabilities of unit cells within each of the delineated optimal exploration target zones is 0.010, which is higher than the average posterior probability (0.0024) of unit cells representing discovered epithermal deposit occurrences (training set 2) and the average posterior probability (0.0029) of unit cells representing (assumed) undiscovered epithermal deposit occurrences (training set 1). These indicate that the algorithm is efficient in finding and selecting optimal exploration focal points in prospective ground. The results also suggest that within the delineated exploration target zones there is much higher probability of mineral deposit occurrence than would be expected due to chance, which is translatable theoretically to increase the chance of a mineral deposit discovery. This suggestion is validated below.

4.5 Prioritization and Validation of Optimal Exploration Target Zones

In practice, exploration target zones are prioritized or ranked according to some criteria. The criteria we applied to prioritize each of the 22 optimal exploration target

zones are (a) the number of prospective pixels and (b) the average posterior probability of prospective pixels. The first criterion represents a measure of whether or not an exploration target zone is wholly made up of prospective cells, whereas the second criterion is an index of mineral occurrence. To each optimal exploration target zone, descending ranks from 1 through to 22 were assigned according to decreasing values per criterion. The ranks per criterion were then added to represent a measure of relative prospectivity; for example, lower sums indicate higher prospectivity. The sums of criteria ranks of each individual exploration target zones were assigned ascending ranks from 22 to 1 indicating their priority for further investigation. Table 3 summarizes the priority/rank derived for each exploration target zone.

In order to validate the derived optimal exploration target zones, the presence of at least one undiscovered deposit occurrence within each of the derived optimal exploration target zones was determined. In addition, the distance from each of the derived optimal exploration target zones to the nearest undiscovered deposit occurrence was determined. The 238 m buffer zones of seven optimal exploration focal points (T01, T02, T05, T08, T10, T13, and T21) contain at least one (assumed) undiscovered deposit occurrence (Table 3). Five of the top 10 priority optimal exploration target zones (T01, T02, T05, T08, and T10) contain at least one (assumed) undiscovered deposit occurrence. The 238 m buffer zones of three optimal exploration focal points (T06, T12, and T16) are only about 10–30 m away from an undiscovered deposit occurrence. However, for the other 12 optimal exploration focal points, whose 238 m buffer zones do not contain an (assumed) undiscovered deposit occurrence and whose buffer limits are at least 50 m away from an (assumed) undiscovered deposit occurrence, the average distance to their corresponding nearest (assumed) undiscovered deposit occurrence is just about 600 m. Figure 6 also shows that all of the nine (assumed) undiscovered deposit occurrences (i.e., those predicted correctly by the input WofE model of mineral prospectivity) are within or very close (on average about 15 m) from a delineated optimal exploration target zone. The other five undiscovered deposit occurrences not predicted by the WofE model (and thus not assumed to be undiscovered deposit occurrences in the derivation of optimal exploration focal points) are, on average, about 230 m away from the limits of an optimal exploration focal point. These results indicate that derived optimal exploration focal points are satisfactorily positioned such that further mineral prospecting within and up to a few tens of meters beyond their 238 m buffer limits could potentially lead to mineral deposit occurrence discovery.

4.6 Discussion on Derivation of Optimal Exploration Target Zones

Until now, there is no objective procedure for demarcating and prioritizing of new exploration target zones based on regional- to district-scale mineral prospectivity maps that have been determined subjectively. That is, portions of predicted prospective ground that are distal to and not containing discovered mineral deposit occurrences are considered, based on subjective judgement, new exploration target zones. In this study, new exploration target zones are determined based on the spatial distribution of estimated posterior probabilities of mineral deposit occurrence, which are used as weights in an objective function in SA to determine optimal exploration focal points. Cross-validation of the results, by using mineral deposit occurrence data, that

Table 3 Results of prioritization and validation of optimal exploration target zones. Rows in bold and italics indicate that target (i.e., buffered) zones around individual optimal exploration focal points that, respectively, contain and are proximal to 30 m of an undiscovered deposit occurrence (i.e., cross-validation deposit occurrence predicted correctly by WofE predictive model of mineral prospectivity)

ID[a]	Prioritization of target zones						Validation of target zones	
	Crit1[b]	Rank1[c]	Crit2[d]	Rank2[e]	SumR12[f]	Final Rank[g]	Within zone[h]	Distance[i]
T01	**237**	**1**	**0.00512**	**1**	**2**	**1**	**Yes**	**159.7**
T02	**222**	**4**	**0.00395**	**4**	**8**	**2**	**Yes**	**33.9**
T03	231	2	0.00370	7	9	3	No	314.6
T04	216	5	0.00376	6	11	4	No	638.9
T05	**226**	**3**	**0.00353**	**9**	**12**	**5.5**	**Yes**	**150.0**
T06	*199*	*9*	*0.00401*	*3*	*12*	*5.5*	*No*	*266.2*
T07	212	7	0.00358	8	15	7	No	334.0
T08	**191**	**11**	**0.00378**	**5**	**16**	**8.5**	**Yes**	**217.8**
T09	186	14	0.00430	2	16	8.5	No	430.8
T10	**215**	**6**	**0.00311**	**13**	**19**	**10**	**Yes**	**222.6**
T11	187	12.5	0.00323	11	23.5	11	No	464.6
T12	*210*	*8*	*0.00255*	*16*	*24*	*12*	*No*	*261.4*
T13	**185**	**15**	**0.00345**	**10**	**25**	**13**	**Yes**	**164.6**
T14	187	12.5	0.00292	15	27.5	14	No	759.9
T15	172	17	0.00318	12	29	15	No	706.6
T16	*196*	*10*	*0.00189*	*21*	*31*	*16*	*No*	*246.8*
T17	142	19	0.00302	14	33	17	No	905.1
T18	180	16	0.00237	18	34	18	No	1021.2
T19	116	20	0.00245	17	37	19.5	No	421.1
T20	143	18	0.00223	19	37	19.5	No	663.1
T21	**106**	**21**	**0.00195**	**20**	**41**	**21**	**Yes**	**150.0**
T22	47	22	0.00069	22	44	22	No	551.8

[a]Target zone ID, with number representing priority

[b]Values for criterion 1 (i.e., number of unit cells with posterior probability > prior probability within each of the 238 m buffered optimal exploration focal points)

[c]Descending ranks assigned to decreasing values for criterion 1

[d]Values for criterion 2 (i.e., average posterior probability of all unit cells within each of the 238 m buffered optimal exploration focal points)

[e]Descending ranks assigned to decreasing values for criterion 2

[f]Sum of ranks for criteria 1 and 2

[g]Ascending ranks assigned to increasing sums of Rank1 and Rank2

[h]Presence of (assumed) undiscovered deposit within the 238 m buffer zone

[i]Distance to the nearest (assumed) undiscovered deposit (m)

were not used to create the probabilistic mineral prospectivity map, suggests that the derived optimal exploration target zones are useful in guiding further exploration towards probable locations of undiscovered mineral deposits. Thus, by application of

the proposed methodology, optimal exploration target zones can be derived objectively, instead of subjectively, from a given probabilistic mineral prospectivity map.

Although we demonstrated our proposed methodology for deriving optimal exploration target zones by using as input a posterior probability map, it can be adapted to accommodate other maps of numerical indices of mineral prospectivity in the range [0, 1]. Examples, such as, fuzzy prospectivity membership values and degrees of evidential belief. Other numerical indices of mineral prospectivity not in the range [0, 1] can be transformed into this range so they can be used as input to our proposed methodology. In addition, a threshold index for differentiating between prospective and non-prospective pixels must be specified so that the optimal exploration focal points are searched and selected in neighborhoods of prospective pixels with index of prospectivity above this threshold. In the present case study, we used the estimated prior probability of mineral deposit occurrence as the threshold index. The graphical technique of Porwal et al. (2003) can be useful in determining threshold indices particularly for knowledge-driven fuzzy approaches that do not involve updating of prior probability of mineral occurrence.

A critical consideration in the application of the objective function in SA is the plausible number of exploration focal points. This number should be at least equal to the number of undiscovered occurrences of mineral deposits. Estimation of undiscovered deposits in geologically-permissive terrane is based on grade-and-tonnage model of deposit-type of interest and is practically performed through consensus by a group of geoscience experts in mineral deposits (Singer and Kouda 1997). We did not perform this exercise because the first criterion is not satisfied, as epithermal mineralizations according to our database are mostly showings or prospects while a few of them are deposits or measured reserves, and that not all of us met the second criterion. Furthermore, we did not estimate the number of undiscovered deposits in the district. As an alternative procedure, we applied the binomial distribution to estimate a plausible number of exploration focal points based on correctly predicted and thus assumed undiscovered cross-validation mineral deposit occurrences. Using an estimated number of exploration focal points based on actually discovered known mineral deposit occurrences illustrates, nonetheless, that our proposed methodology provides a potentially useful link between predictive modeling of mineral prospectivity and assessment of undiscovered mineral resources. For example, if number of undiscovered deposits and their corresponding confidence or probability levels have been estimated (Cox 1993; Singer 1994; Scott and Dimitrakopoulous 2001; McCammon et al. 2004) then such estimates could be used, respectively, in lieu of r and 0.95 in (14). For p in (14), we have shown that using the prediction rate of a mineral prospectivity model results in a plausible number of exploration focal points. If all discovered mineral deposit occurrences would be used for modeling of mineral prospectivity, then p in (14) could be represented by the success or fitting rate of a mineral prospective model (i.e., proportion of training deposit occurrences coinciding with prospective pixels or values in a predictive model). In this case, estimates of the number of undiscovered mineral deposit occurrences and their corresponding confidence or probability levels should be obtained in order to estimate the number of exploration focal points.

In district-scale mineral prospectivity mapping, one does not aim to define drilling targets as individual pixels but as prospective zones defined by a neighborhood of

pixels of high prospectivity for further exploration work. Therefore, after deriving optimal exploration focal points as individual pixels based on a probabilistic mineral prospectivity map, we defined exploration target zones around them. The analysis presented is based upon available datasets and geo-information derived from them, but avoids subjective expert opinion. As an alternative analysis, we have also studied the spatial support around the derived optimal exploration focal points based on the variography of random samples of posterior probabilities in the central part of the study area where most of the known epithermal deposits occur (Fig. 5b). In this alternative analysis, we encountered two problems. First, the number of random samples of posterior probabilities was inadequate to define a meaningful spatial pattern. Second, the variograms were mostly showing a pure nugget, which is probably due to an inadequacy of numbers of random samples of posterior probabilities or the discretization of evidential data into binary maps in the WofE modeling. Delineation of optimal exploration target zones around derived optimal exploration focal points apparently needs further research.

The best way to validate the proposed methodology for guiding mineral prospecting to undiscovered deposit occurrences is to visit and perform detailed sampling and prospecting work in the delineated and prioritized optimal exploration target zones. The way forward as shown in our study is to further test the proposed methodology in control areas where works on both mineral prospectivity modeling and assessment of undiscovered mineral resources has already been carried out.

5 Conclusions

This study resulted in three main conclusions.

- The proposed methodology provides for objectively, and with reasonable accuracy, demarcation and selection of optimal exploration target zones for further investigation of undiscovered mineral deposit occurrences based on a given probabilistic mineral prospectivity map. In the study area, nine out of 14 (assumed) undiscovered epithermal deposit occurrences, predicted correctly by a WofE predictive model of mineral prospectivity, are either within or at most 30 m away from a buffered zone of an optimal exploration focal point.
- The analysis described for deriving optimal exploration focal points in order to demarcate and prioritize exploration target zones is shown to be useful in this study. Further work, however, is needed to test and/or improve the analysis and to test other approaches.
- Airborne hyperspectral images provide valuable information for predictive modeling of prospectivity for epithermal deposits in the study area, particularly if they are supported by other pieces of spatial evidence, such as proximity to faults and fractures.

Acknowledgements The authors would like to acknowledge thanks to the sponsors of this work, namely, ITC International Institute for Geo-Information Science and Earth Observation, project number 3083022 and NRF National Research Foundation SA, project number 10317, gun 2053944.

References

Abrams M, Ashley R, Rowan L, Goetz AFH, Kahle A (1977) Use of imaging in the .46–2.36 μm spectral region for alteration mapping in the Cuprite mining district. Nevada: USGS OFR-77-585

Agterberg FP (1992) Combining indicator patterns in weights of evidence modeling for resource evaluation. Nonrenew Resour 1(1):39–50

Agterberg FP, Bonham-Carter GF (1999) Logistic regression and weights of evidence modeling in mineral exploration. In: Proceedings of 28th international symposium on computer applications in the mineral industries, pp 483–590

Agterberg FP, Bonham-Carter GF (2005) Measuring the performance of mineral-potential maps. Nat Resour Res 14(1):1–17

Agterberg FP, Cheng W (2002) Conditional independence test of weights-of-evidence modeling. Nat Resour Res 11(4):249–255

Agterberg FP, Bonham-Carter GF, Wright DF (1990) Statistical pattern integration for mineral exploration. In: Gaal G, Merriam DF (eds) Computer applications in resource exploration and assessment for minerals and petroleum. Pergamon, Elmsford, pp 1–21

Arribas A (Jr), Cunningham CG, Rytuba JJ, Rye RO, Kelley WC, Podwysocki MH, McKee EH, Tosdal RM (1995) Geology, geochronology, fluid inclusions, and isotope geochemistry of the Rodalquilar gold alunite deposit, Spain. Econ Geol 90:795–822

Bishop MM, Fienberg SE, Holland PW (1975) Discrete multivariate analysis: theory and practice. MIT Press, Cambridge, 587 p

Bohachevsky IO, Johnson ME, Stein ML (1986) Generalized simulated annealing for function optimization. Technometrics 28(3):209–217

Bonham-Carter GF, Agterberg FP, Wright DF (1988) Integration of geological datasets for gold exploration in Nova Scotia. Photogramm Eng Remote Sens 54:1585–1592

Bonham-Carter GF, Agterberg FP, Wright DF (1989) Weights of evidence modelling: a new approach to mapping mineral potential. In: Agterberg FP, Bonham-Carter GF (eds) Statistical applications in the Earth sciences: geological survey. Canada paper 89-9, pp 171–183

Boots BN, Getis A (1988) Point pattern analysis. Sage university scientific geography series, vol 8. Sage, Thousand Oaks, 93 p

Carranza EJM, Hale M (2000) Geologically constrained probabilistic mapping of gold potential, Baguio district, Philippines. Nat Resour Res 9(3):237–253

Carranza EJM, Hale M (2003) Evidential belief functions for data-driven geologically constrained mapping of gold potential, Baguio district, Philippines. Ore Geol Rev 22(1):117–132

Chung CF, Agterberg FP (1980) Regression models for estimating mineral resources from geological map data. Math Geol 12(5):473–488

Clark RN, Swayze GA, Gallagher AJ, King TVV, Calvin WM (1993) The US geological survey, digital spectral library: Version 1: 0.2 to 3.0 microns. US Geological Survey Open File Report, pp 93–592

Cox DP (1993) Estimation of undiscovered deposits in quantitative mineral resource assessments examples from Venezuela and Puerto Rico. Nonrenew Res 2(2):82–91

Crósta AP, de Souza-Filho CR, Azevedo F, Brodie C (2003) Targeting key alteration minerals in epithermal deposits in Patagonia, Argentina, using ASTER imagery and principal component analysis. Int J Remote Sens 24(21):4233–4240

Cudahy T, Okada K, Brauhart C (2000) Targeting VMS-style Zn mineralisation at Panorama, Australia, using airborne hyperspectral VNIR-SWIR HyMap data. In: ERIM proceedings of the 14th international conference on applied geologic remote sensing, Las Vegas, pp 395–402

de Gruijter JJ, ter Braak CJF (1990) Model-free estimation from spatial samples: a reappraised of classical sampling theory. Math Geol 22(4):407–415

Debba P, van Ruitenbeek F, van der Meer F, Carranza EJM, Stein A (2005) Optimal field sampling for targeting minerals using hyperspectral data. Remote Sens Environ 99(4):373–386

Debba P, Stein A, van der Meer F, Carranza EJM, Lucieer A (2008) Field sampling from a segmented image. In: Gervasi O, Murgante B, Laganá A, Taniar D, Mun Y, Gavrilova ML (eds) Computational science and its applications ICCSA 2008. Series LNCS, vol 5072. Springer, Heidelberg, pp 756–768. ISBN 978-3-540-69838-8

Goetz AFH, Srivastava V (1985) Mineralogical mapping Cuprite mining district, Nevada. In: Vane G, Goetz A (eds) Proc Airborne imaging spectrometer data analysis workshop. Jet propulsion laboratory publication 85-41. Jet Propulsion Laboratory, Pasadena, pp 22–31

Good IJ (1950) Probability and the weighing of evidence. Griffin, London, 119 p

IGME (1981) Mapa Geologico de España (Carboneras, 1.046/24–43; El Pozo de los Frailes, 1.060/24–44), e. 1:50,000. Instituto Geologico y Minero de España (IGME), Servicio de Publicaciones, Ministerio de Industria y Energia, Madrid

Kirkpatrick S, Gelatt CD (Jr), Vecchi MP (1983) Optimization by simulated annealing. Science 220(4598):671–680

Kruse FA (2002) Comparison of AVIRIS and Hyperion for hyperspectral mineral mapping. In: SPIE aerospace conference, 9–16 March 2002, Big Sky, Montana. Published on CD-ROM, IEEE Catalog Number 02TH8593C, Paper 6.0102, pp 1–12

Lillesand TM, Kiefer RW, Chipman JW (1994) Remote sensing and image interpretation. Wiley, New York, 750 p

McCammon RB, Root DH, Schruben PG (2004) Statewide estimates of undiscovered deposits of gold, silver, copper, lead, and zinc. Nat Resour Res 13(3):201–207

Pan G (1993) Canonical favorability model for data integration and mineral potential mapping. Comput Geosci 19(8):1077–1100

Porwal A, Carranza EJM, Hale M (2003) Artificial neural networks for mineral-potential mapping: a case study from Aravallia province, Western India. Nat Resour Res 12(3):155–171

Richter R (1996) Atmospheric correction of DAIS hyperspectral image data. In: SPIE proceedings, vol 2756. Int Soc Opt Eng, Bellingham, pp 390–399

Rigol-Sanchez JP, Chica-Olmo M, Abarca-Hernandez F (2003) Artificial neural networks as a tool for mineral potential mapping with GIS. Int J Remote Sens 24(5):1151–1156

Scott M, Dimitrakopoulous R (2001) Quantitative analysis of mineral resources for strategic planning: implications for Australian geological surveys. Nat Resour Res 10(3):159–177

Singer DA (1993) Basic concepts in three-part quantitative assessments of undiscovered mineral resources. Nonrenew Resour 2(2):69–81

Singer DA (1994) Conditional estimates of the number of podiform chromite deposits. Nonrenew Resour 3(3):200–204

Singer DA, Kouda R (1997) Classification of mineral deposits into types using mineralogy with a probabilistic neural network. Nonrenew Res 6(1):27–32

Singer DA, Kouda R (2003) Typing mineral deposits using their grades and tonnages in an artificial neural network. Nat Resour Res 12(3):201–208

Shyan-Shu S, Ji-Zheng C, Shi-Shang J (2005) An interactive sampling strategy based on information analysis and ordinary kriging for locating hot spot regions. Math Geol 37(1):29–48

Tapia R, Stein A, Bijker W (2005) Optimization of sampling schemes for vegetation mapping using fuzzy classification. Remote Sens Environ 99(4):425–433

Thiart C, Bonham-Carter GF, Agterberg FP, Cheng Q, Panahi A (2004) An application of the new omnibus test for conditional independence in weights-of-evidence modeling. In: Harris J, Wright D (eds) Special volume on GIS applications in the Earth sciences. Geological Association of Canada, Calgary (chapter in book in press)

van Groenigen JW, Gandah M, Bouma J (2000a) Soil sampling strategies for precision agriculture research under Sahelian conditions. Soil Sci Soc Am J 64:1674–1680

van Groenigen JW, Pieters G, Stein A (2000b) Optimizing spatial sampling for multivariate contamination in urban areas. Environmetrics 11:227–244